1494–1507 *Nucleic Acids Research, 2020, Vol. 48, No. 3* *Published online 8 December 2019*
doi: 10.1093/nar/gkz1143

LGP2 virus sensor enhances apoptosis by upregulating apoptosis regulatory genes through TRBP-bound miRNAs during viral infection

Tomoko Takahashi [1], Yuko Nakano[1], Koji Onomoto[2], Mitsutoshi Yoneyama[2] and Kumiko Ui-Tei [1,3,*]

[1]Department of Biological Sciences, Graduate School of Science, The University of Tokyo, Tokyo 113-0033, Japan, [2]Division of Molecular Immunology, Medical Mycology Research Center, Chiba University, Chiba 260-8673, Japan and [3]Department of Computational Biology and Medical Sciences, Graduate School of Frontier Sciences, The University of Tokyo, Chiba 277-8561, Japan

Received August 28, 2019; Revised November 16, 2019; Editorial Decision November 18, 2019; Accepted November 27, 2019

ABSTRACT

During viral infection, viral nucleic acids are detected by virus sensor proteins including toll-like receptor 3 or retinoic acid-inducible gene I-like receptors (RLRs) in mammalian cells. Activation of these virus sensor proteins induces type-I interferon production and represses viral replication. Recently, we reported that an RLR family member, laboratory of genetics and physiology 2 (LGP2), modulates RNA silencing by interacting with an RNA silencing enhancer, TAR-RNA binding protein (TRBP). However, the biological implications remained unclear. Here, we show that LGP2 enhances apoptosis by upregulating apoptosis regulatory genes during viral infection. Sendai virus (SeV) infection increased LGP2 expression approximately 900 times compared to that in non-virus-infected cells. Then, the induced LGP2 interacted with TRBP, resulting in the inhibition of maturation of the TRBP-bound microRNA (miRNA) and its subsequent RNA silencing activity. Gene expression profiling revealed that apoptosis regulatory genes were upregulated during SeV infection: caspases-2, -8, -3 and -7, four cysteine proteases with key roles in apoptosis, were upregulated directly or indirectly through the repression of a typical TRBP-bound miRNA, miR-106b. Our findings may shed light on the mechanism of apoptosis, induced by the TRBP-bound miRNAs through the interaction of TRBP with LGP2, as an antiviral defense system in mammalian cells.

INTRODUCTION

RNA silencing is a posttranscriptional gene silencing mechanism directed by microRNAs (miRNAs), non-coding RNAs of ∼21–22 nucleotides (nt) in length that are conserved in diverse organisms (1). The human genome encodes >2000 miRNAs that regulate the expression of multiple genes (2). Primary miRNAs transcribed from the genome are processed into precursor-miRNAs (pre-miRNAs) by an endoribonuclease, Drosha, in the nucleus (3–5). Pre-miRNAs are exported into the cytoplasm by exportin (6,7), and are further processed by another endoribonuclease, Dicer, into miRNA duplexes with 2-nt 3′ overhangs (8). One strand of the miRNA duplex is loaded onto Argonaute (AGO), a main component of the RNA-induced silencing complex, resulting in destabilization or translational repression of target mRNAs with sequence complementarities (9,10). TAR-RNA binding protein (TRBP) is a double-stranded RNA (dsRNA) binding protein identified as a factor that binds to human immunodeficiency virus type 1 TAR RNA (11), and functions as an RNA silencing enhancer (12,13). TRBP binds to the stem region of pre-miRNA and recruits Dicer to enhance miRNA maturation (14). In our previous report, we revealed that TRBP has a binding preference for a specific type of pre-miRNAs whose stem has tight base-pairing, resulting in selective regulation of their target gene expression (15).

During viral infection, viral RNAs are recognized as exogenous RNAs by viral sensor proteins and activate the antiviral innate immune response (16,17). Toll-like receptor 3 (TLR3) and retinoic acid-inducible gene I (RIG-I)-like receptors (RLRs), including RIG-I (or DDX58), melanoma-differentiation-associated gene 5 (MDA5 or IFIH1), and laboratory of genetics and physiology 2 (LGP2 or DHX58), are representative sensors for viral RNAs in the endosome and cytoplasm, respectively (18–20). When RIG-I recognizes 5′-triphosphate- or 5′-diphosphate-containing RNA

*To whom correspondence should be addressed. Tel: +81 3 5841 3044; Fax: +81 3 5841 3044; Email: ktei@bs.s.u-tokyo.ac.jp

and small RNA duplexes (21–25), or MDA5 recognizes long RNA duplexes as exogenous RNAs (26), they transfer signals to downstream molecules through their caspase recruitment domains (CARDs) (27–29). Activation of the signaling cascade induces type-I interferon (IFN) production and the secreted IFN upregulates hundreds of IFN-stimulated genes (ISGs), resulting in the inhibition of viral replication (16). LGP2 is a member of the RLRs, but does not have a CARD, rendering it incapable of transferring signals downstream. Thus, the function of LGP2 was unclear.

Recently, we reported that LGP2 modulates RNA silencing by interacting with the RNA silencing enhancer, TRBP (15). LGP2 interacts with TRBP via the dsRNA-binding sites of TRBP through competition with TRBP-bound pre-miRNAs. This competitive binding inhibits the binding of 40 types of pre-miRNAs with TRBP in HeLa cells, as well as the maturation of those miRNAs by Dicer/TRBP, and their subsequent RNA silencing activities (15). Thus, LGP2 has been demonstrated to inhibit RNA silencing directed by TRBP-bound miRNAs and upregulate expression of their target genes (15). However, the biological implications of this activity remained unclear.

Here, we show that LGP2 upregulated apoptosis regulatory genes by inhibition of TRBP-bound pre-miRNA maturation by competitive binding with TRBP, and enhanced apoptosis during Sendai virus (SeV) infection. SeV is a single-stranded RNA virus recognized by RIG-I, and its infection induces IFN production, which strongly induces LGP2 expression. Induced LGP2 protein interacted with TRBP and reduced RNA silencing directed by a typical TRBP-bound miRNA, miR-106b, resulting in upregulation of its target genes, including initiator or executioner caspases, directly or indirectly. Our finding showed that the crosstalk between RNA silencing and RLR signaling functions to induce apoptosis as an antiviral defense system in mammalian cells.

MATERIALS AND METHODS

Cell culture

Human HeLa wild-type (WT), LGP2$^{-/-}$ or TRBP$^{-/-}$ cells (15) were cultured in Dulbecco's Modified Eagle's Medium (Wako, Osaka, Japan) containing 10% fetal bovine serum (Biowest, Nuaillé, France) and antibiotics [100 U/ml of penicillin and 100 μg/ml of streptomycin (Sigma-Aldrich, St Louis, MO, USA)] at 37°C with 5% CO_2.

Plasmid construction

The expression plasmids containing N-terminal FLAG-tagged TRBP (pcDNA5-FLAG-TRBP) or miR-106b inhibitor (pTuD-miR-106b) were constructed as described previously (15). For construction of endogenous miRNA activity sensor plasmids (psiCHECK-miR-106b, or -19b), oligonucleotides with target sequences complementary to each miRNA (miR-106b, or -19b) were chemically synthesized with *Xho*I/*Eco*RI ends. The resultant dsDNAs were inserted into the XhoI/EcoRI site in the 3′ untranslated region (3′UTR) of *Renilla* luciferase in psiCHECK-1 (Promega, Madison, WI, USA). For construction of reporter plasmids encoding the *Renilla* luciferase coding region (CDS) with the entire 3′UTR of caspase-2 or -8 (psiCHECK-CASP2-3′UTR-WT or psiCHECK-CASP8-3′UTR-WT), the 3′UTR fragment of caspase-2 or -8 with XhoI/EcoRI ends was amplified using cDNA synthesized from total RNA extracted from HeLa WT cells. Each of the resultant DNA fragments was inserted separately into the *Xho*I/*Eco*RI site in the 3′UTR of *Renilla* luciferase in psiCHECK-1 (Promega). For construction of plasmids with mutated miR-106b target sites (psiCHECK-CASP2-3′UTR-mt or psiCHECK-CASP8-3′UTR-mt), miR-106b target sites were predicted by seed sequence complementarity and three nucleotides were deleted from the predicted sites by site-directed mutagenesis using KOD One PCR Master Mix (Toyobo, Osaka, Japan). The construct was purified using the Genopure Plasmid Midi Kit (Roche, Basel, Switzerland). The oligonucleotide sequences used for plasmid construction are shown in Supplementary Table S1.

Viral infection

Newcastle disease virus (NDV, Miyadera strain), Sendai virus (SeV, Cantell strain), or Influenza A virus (IAV, PR8 strain) was incubated with serum-free medium for 1 h at 37°C. After adsorption, the medium was changed and the cells were cultured in serum-containing medium at 37°C with 5% CO_2 with or without 30 μM benzyloxycarbonyl-Val-Ala-Asp-fluoromethylketone (z-VAD-FMK; Peptide institute. Inc., Osaka, Japan). The non-structural protein 1 (NS1) of IAV is usually known as an RNAi repressor, but the IAV strain we used is known as a non-RNA silencing repressor (30).

Quantitative reverse transcription (qRT)-PCR

Total RNA was extracted using the FastGene RNA Premium Kit (Nippon Genetics, Tokyo, Japan). The extracted RNA (0.5 μg) was used for cDNA synthesis with the High-Capacity cDNA Reverse Transcription Kit (Applied Biosystems, Foster City, CA, USA). qRT-PCR was performed using the KAPA SYBR Fast qPCR Master Mix ABI Prism Kit (Kapa Biosystems, Wilmington, MA, USA) with the StepOnePlus Real-Time PCR System (Applied Biosystems). For the detection of mature or precursor miRNAs, total RNA including small RNAs was extracted using the FastGene RNA Premium Kit with FastGene miRNA enhancer. The extracted RNA (0.5 μg) was used for cDNA synthesis using specific stem–loop RT primers. The primer sequences are shown in Supplementary Table S2.

Western blot

The samples were separated by sodium dodecyl sulfate polyacrylamide gel electrophoresis (SDS-PAGE) and transferred to a polyvinylidene fluoride membrane using the Trans-Blot Turbo Transfer System (Bio-Rad, Hercules, CA, USA). The membrane was blocked for 1 h in Tris-buffered saline-Triton X-100 or Tween 20 (TBS-T; 20 mM Tris–HCl [pH 7.5], 150 mM NaCl, 0.2% Triton X-100 or 0.1% Tween) supplemented with 5% skim milk (Wako), and incubated with specific antibodies in Can Get Signal immunoreaction enhancer solution (Toyobo) at 4°C overnight. Anti-TRBP (AbFrontier, Seoul, Korea), anti-AGO2 (Wako),

anti-PKR (Santa Cruz Biotechnology, Dallas, TX, USA), anti-phospho PKR (Abcam, Cambridge, UK), anti-FLAG (Cell Signaling, Danvers, MA, USA) and anti-α-tubulin antibodies (Abcam) were used. Anti-human RIG-I, anti-MDA5, anti-LGP2, and anti-Dicer antibodies were generated by immunizing rabbits with a synthetic peptide (8,31). The membranes were washed three times with TBS-T and reacted with HRP-linked anti-rabbit or anti-mouse antibody (GE Healthcare, Chicago, IL, USA) at room temperature for 1 h. After being washed three times with TBS-T, the membrane was incubated with ECL Prime Western Blotting Detection Reagent (GE Healthcare) and visualized using the ImageQuant LAS 4000 Mini imager (GE Healthcare).

Immunoprecipitation

A HeLa cell suspension (5×10^5 cells/well) was plated into a six-well plate 1 day before transfection. Cells were washed with phosphate-buffered saline and lysed in cold lysis buffer (10 mM HEPES–NaOH [pH 7.9], 1.5 mM $MgCl_2$, 10 mM KCl, 0.5 mM DTT, 140 mM NaCl, 1 mM EDTA, 1 mM Na_3VO_4, 10 mM NaF, 0.5% NP-40 and complete protease inhibitor) 14 h following viral infection, then the cell lysates were centrifuged at 14 000 rpm for 10 min. For immunoprecipitation, 30 μl of Protein G Agarose (Merck Millipore, Burlington, MA, USA) was mixed with 2.5 μg of mouse anti-FLAG antibody (Sigma, St Louis, MO, USA), or 2.5 μg of mouse IgG (Santa Cruz Biotechnology) as a negative control and rotated at 4°C for 2 h. The cell lysates were then added to antibody-bound Protein G Agarose and rotated at 4°C for 2 h. The beads were washed twice with wash buffer containing 300 mM NaCl and once with lysis buffer. To elute the bound proteins, 2× SDS-PAGE sample buffer (30 μl) was added and the beads were boiled for 5 min.

Northern blot

A HeLa cell suspension (2.7×10^6 cells/dish) was plated into a 9-cm dish 1 day before viral infection. RNA extraction was performed using ISOGEN reagent (Nippon Gene, Tokyo, Japan) 14 h following viral infection. Total RNA (20 μg) was loaded onto a 10% denatured polyacrylamide gel containing 8 M urea and transferred to an Amersham Hybond-N+ membrane (GE Healthcare) at 25 V for 45 min. The membrane was hybridized with ^{32}P-labeled DNA probe at 37°C overnight following crosslinking and prehybridization. The membranes were washed three times at 37°C and visualized using a Typhoon FLA 9500 imager (GE Healthcare). The probe sequences are shown in Supplementary Table S3.

RNA silencing activity assay for endogenous miRNAs

RNA silencing activity was measured with a luciferase reporter assay. To measure the RNA silencing activity of endogenous miR-106b or -19b, a HeLa cell suspension (1.0×10^5 cells/ml) was inoculated in 24-well plates 1 day before transfection. Cells were transfected with 0.25 μg of psiCHECK-1 vector (Promega) encoding the complementary sequence of miR-106b or miR-19b in the 3′UTR of *Renilla* luciferase and 0.5 μg of pGL3-Control encoding the firefly luciferase gene with polyethylenimine. Viral infection was performed 1 day following transfection, and the cells were lysed with 1× passive lysis buffer (Promega) 14 h following viral infection. Luciferase activity was measured using the Dual-Luciferase Reporter Assay System (Promega), and the *Renilla* luciferase activity normalized to that of firefly luciferase (*Renilla* luciferase activity/firefly luciferase activity) was determined.

Microarray analysis

Human HeLa WT, LGP2$^{-/-}$ or TRBP$^{-/-}$ cells were collected at 14 h following viral infection. Total RNA was extracted using the RNeasy Mini Kit (Qiagen, Hilden, Germany) and treated with DNase I (Qiagen). The quality of the total RNA was confirmed using a Bioanalyzer (Agilent Technologies, Santa Clara, CA, USA), and cDNA and Cy-3-labeled RNA were synthesized using the Quick Amp Labeling kit for One Color (Agilent Technologies). Cy-3-labeled RNAs were fragmented using the Gene Expression Hybridization Kit (Agilent Technologies) and hybridized to a SurePrint G3 Human GE Microarray version 3 (Agilent Technologies) at 65°C for 17 h. After being washed, the microarray slide was scanned by a DNA Microarray Scanner (Agilent Technologies) and the signals were quantified by Feature Extraction 10.5.1.1 software (Agilent Technologies). Data analysis was performed on probes that passed filtering and gene ontology (GO) analysis was performed by the DAVID online software tool (32,33).

Cell viability assay

A HeLa cell suspension (0.5×10^5 cells/ml) was inoculated in 24-well plates 1 day before viral infection. Cells were collected in Trypsin-EDTA (Wako) and stained with 0.4% (w/v) Trypan Blue Solution (Wako). Cell counting was performed using a TC20 Automated Cell Counter (Bio-Rad), and the cell viabilities of virus-infected cells normalized to that of mock-treated cells were determined.

RESULTS

SeV infection induces LGP2 expression

Recently, we reported that LGP2, a member of the RLR family, functions as an RNA silencing modulator by interacting with TRBP, an RNA silencing enhancer. This interaction results in the inhibition of pre-miRNA binding with TRBP, miRNA maturation by Dicer/TRBP, and subsequent RNA silencing activities directed by TRBP-bound miRNAs (15). The expression of LGP2 protein is low in non-virus-infected cells, while its expression is induced by positive feedback regulation through the secreted IFN during viral infection. To reveal the biological implications of modulation of RNA silencing by LGP2 upregulation, we first looked for a virus whose infection could induce abundant expression of LGP2. We infected HeLa WT and LGP2$^{-/-}$ cells with NDV, SeV or IAV. These viruses are negative-sense single-stranded RNA viruses recognized by RIG-I. NDV and SeV are included in the family Paramyxoviridae, and IAV is included in the family Orthomyxoviridae. The mock-treated or virus-infected cells were collected

at 0, 6, 10, 14, 18 and 24 h following the infection. qRT-PCR analysis showed that NDV and SeV infection induced IFN-β mRNA up to 15 000 fold at 18 h and 300–400 fold at 6 h following infection, respectively (Figure 1A). However, IFN-β mRNA was not increased by IAV infection, because IAV inhibits IFN production by its NS1 protein (31,34). Furthermore, the increased levels of IFN-β mRNA showed no significant differences between WT and LGP2$^{-/-}$ cells during NDV or SeV infection, indicating that type-I IFN signaling was activated during NDV or SeV infection regardless of LGP2 expression (Figure 1A). Western blot analysis showed that the expression of LGP2 protein was evident from 10 h and increased until 14 h or later by SeV infection, whereas LGP2 expression was not induced by NDV or IAV infection (Figure 1B). Similarly, RIG-I and MDA5 proteins were increased by SeV infection but not by NDV or IAV infection. IAV did not produce IFN, therefore it could not induce LGP2, RIG-I and MDA5 expression. NDV infection certainly increased IFN-β production, but it also induced phosphorylation of dsRNA-dependent protein kinase (PKR) in both WT and LGP2$^{-/-}$ cells (Figure 1B). The phosphorylation of PKR induces phosphorylation of eukaryotic initiation factor 2α, which is involved in the initiation phase of translation (35,36), and its phosphorylation blocks *de novo* protein synthesis. Thus, among these RNA viruses, we chose SeV, which is able to produce IFN and induce abundant expression of LGP2 protein as well as RIG-I and MDA5.

LGP2 interacts with TRBP and reduces RNA silencing during SeV infection

As shown in Figure 1B, SeV induced the abundant expression of LGP2 protein at 14 h following infection. Western blot analysis using cell lysate at 14 h following SeV infection showed that the expression levels of RLRs (LGP2, RIG-I and MDA5) were markedly increased, whereas those of RNA silencing factors (TRBP, Dicer and AGO2) did not change (Figure 2A).

To examine whether the upregulated LGP2 interacts with TRBP during SeV infection, either SeV or IAV (negative control) was used to infect WT cells expressing FLAG-tagged TRBP or EGFP (negative control). Then, immunoprecipitation was performed with anti-FLAG antibody at 14 h following infection (Figure 2B). The results revealed that LGP2 was clearly immunoprecipitated with TRBP during SeV infection, but not during IAV infection (Figure 2B and C). Dicer, which is known to interact with TRBP (37), was immunoprecipitated with TRBP regardless of infection with SeV or IAV, although the amount of immunoprecipitated Dicer was decreased during SeV infection (Figure 2B and C). This result indicated that TRBP/LGP2 interaction may disturb not only pre-miRNA binding with TRBP (15), but also TRBP-Dicer interaction. By contrast, RIG-I and MDA5 were not co-immunoprecipitated with TRBP (Figure 2B). Furthermore, it was revealed that endogenous TRBP was certainly immunoprecipitated with LGP2 during SeV infection (Supplementary Figure S1).

Next, we examined whether LGP2 modulates RNA silencing by interacting with TRBP during SeV infection. LGP2 interacts competitively with TRBP through the dsRNA binding site of TRBP, resulting in the reduction of pre-miRNA binding with TRBP, maturation of TRBP-bound pre-miRNAs, and their subsequent RNA silencing activities (15). miR-106b and miR-19b are representative TRBP-bound and non-TRBP-bound miRNAs, respectively (15). Our previous report showed that the amount of mature miR-106b, but not miR-19b, was decreased by LGP2 overexpression, and increased in LGP2$^{-/-}$ cells compared to that in WT cells (15). Furthermore, the expression levels of their target genes were correlated negatively with the expression levels of mature miRNAs (15). To examine whether the induction of LGP2 decreases the expression level of mature miR-106b during SeV infection, we performed northern blot analysis using mock-treated or SeV-infected WT or LGP2$^{-/-}$ cells. Northern blot analysis showed that the mature miR-106b was decreased in WT cells, but not in LGP2$^{-/-}$ cells, during SeV infection (Figure 2D). By contrast, the expression levels of miR-19b were almost unchanged in WT or LGP2$^{-/-}$ cells (Figure 2D). In addition to northern blot analysis, we performed qRT-PCR to quantify the mature and precursor levels of these miRNAs (Figure 2E). The results showed that the mature miR-106b level was significantly decreased in WT cells, but not in LGP2$^{-/-}$ cells, during SeV infection, consistent with the results of northern blot analysis. Furthermore, the precursor miR-106b level was significantly increased in WT cells, but not in LGP2$^{-/-}$ cells. By contrast, the expression levels of the mature and precursor miR-19b were almost unchanged in both WT and LGP2$^{-/-}$ cells. The RNA silencing activities of miR-106b and miR-19b were measured by luciferase reporter assay (Figure 2F). The sensor plasmid for measuring each miRNA activity, encoding the target sequence of miR-106b or miR-19b in 3′UTR of *Renilla* luciferase, was transfected with a plasmid encoding firefly luciferase (internal control) into WT or LGP2$^{-/-}$ cells. The cells were collected at 14 h following SeV or IAV infection, and *Renilla* luciferase activities normalized to firefly luciferase activities (*Renilla* luciferase/firefly luciferase) were determined. Usually NS1 protein of IAV is known as an RNAi repressor, but the type of NS1 protein produced by the IAV strain used in this study has been shown to be a non-RNA silencing repressor (30). The results showed that SeV infection, but not IAV infection, increased the relative luciferase activity by the endogenous miR-106b in WT cells. This means that RNA silencing activity directed by endogenous miR-106b was repressed in WT cells, but not in LGP2$^{-/-}$ cells (Figure 2F, left panel). By contrast, RNA silencing activity directed by endogenous miR-19b showed no significant difference in either WT or LGP2$^{-/-}$ cells (Figure 2F, right panel). Thus, these results suggest that the LGP2 induced by the secreted IFN interacted with TRBP and decreased the mature miR-106b level by decreasing its processing, thereby reducing its subsequent RNA silencing activity during SeV infection.

LGP2-TRBP interaction upregulates apoptosis regulatory genes during SeV infection

To identify the genes whose expression patterns were modulated during SeV infection, we performed gene expression profiling by microarray analysis in mock-treated or SeV-infected WT, LGP2$^{-/-}$ or TRBP$^{-/-}$ cells. MA plots show-

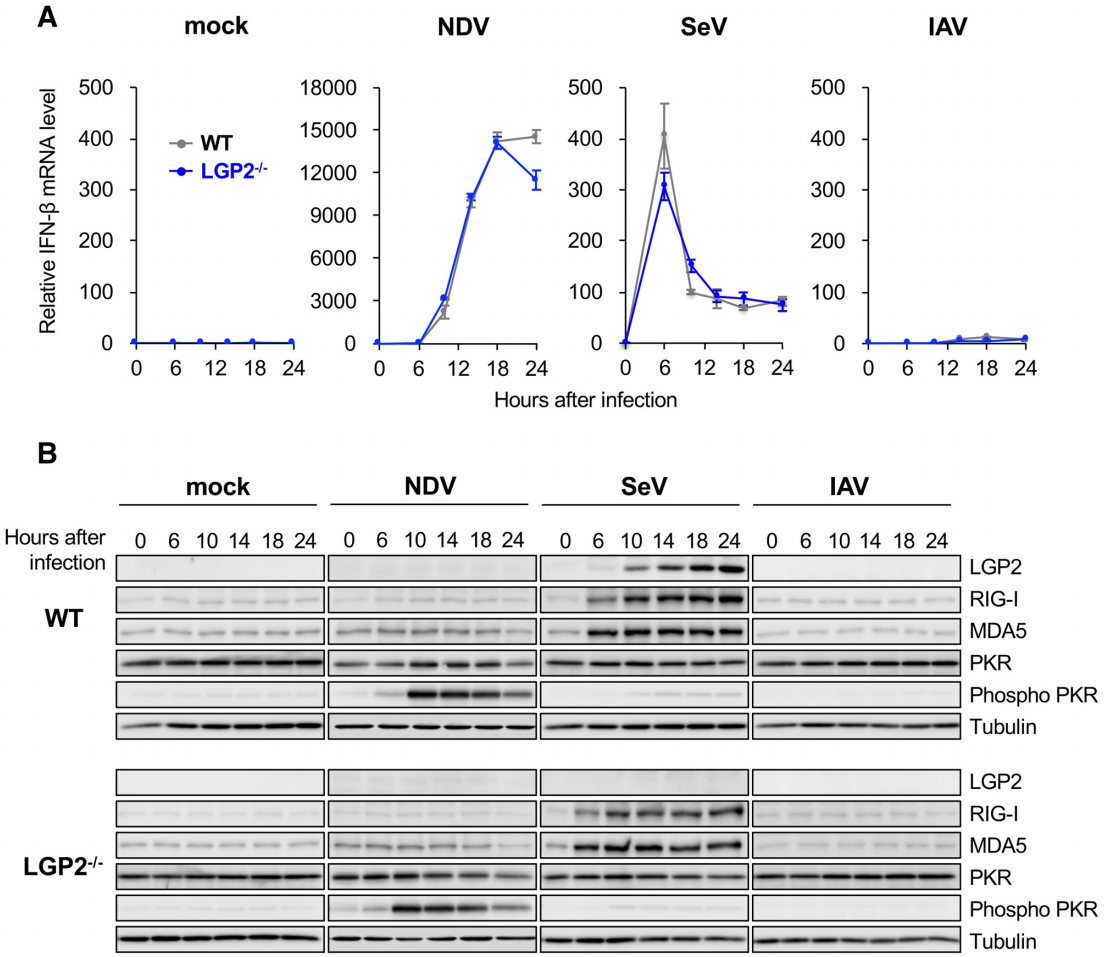

Figure 1. SeV infection induces abundant expression of LGP2. (**A**) Relative mRNA levels of IFN-β in mock-treated or virus (NDV, SeV or IAV)-infected WT or LGP2$^{-/-}$ cells as quantified by qRT-PCR. The cells were collected at 0, 6, 10, 14, 18 and 24 h following virus infection. The experiments were performed in triplicate. (**B**) Western blot of endogenous LGP2, RIG-I, MDA5, PKR, phospho PKR or tubulin using mock-treated or virus (NDV, SeV or IAV)-infected WT or LGP2$^{-/-}$ cells.

ing the $\log_2$ fold-change of signal intensities in SeV-infected cells relative to mock-treated cells (M value, vertical axis) and the averaged $\log_{10}$ signal intensities in mock-treated and SeV-infected cells (A value, horizontal axis), are shown with colors indicating upregulated (SeV/mock $>$ 1.5) or downregulated (SeV/mock $<$ 0.66) transcripts during SeV infection (Figure 3A). The expression levels of RLRs (LGP2, RIG-I and MDA5) were clearly increased during SeV infection, while little or no changes were observed for RNA silencing factors (TRBP, Dicer and AGO2) (Figure 3A). Interestingly, the expression level of LGP2 showed the most remarkable increase in WT cells during SeV infection (fold change [$\log_2$] = 9.9) (Figure 3A, left panel), suggesting that LGP2 has the important function during SeV infection. Venn diagrams show the common and unique upregulated (Figure 3B) or downregulated (Supplementary Figure S2A) transcripts in WT, LGP2$^{-/-}$ and TRBP$^{-/-}$ cells. In total, 667 transcripts were commonly upregulated in all cells, whereas 350, 284 and 137 transcripts were upregulated only in WT, LGP2$^{-/-}$ and TRBP$^{-/-}$ cells, respectively (Figure 3B). By contrast, 711 transcripts were commonly downregulated in all cells, whereas 531, 222 and 206 transcripts were downregulated only in WT, LGP2$^{-/-}$, and TRBP$^{-/-}$ cells, respectively (Supplementary Figure S2A). GO analysis revealed that the 667 commonly upregulated transcripts were enriched in the GO terms related to antiviral innate immune response: defense response to virus, type-I interferon signaling pathway, and negative regulation of viral genome replication (Figure 3C and Supplementary Table S4). These results indicated that the innate immune response was commonly induced in WT, LGP2$^{-/-}$ and TRBP$^{-/-}$ cells during SeV infection. It has been reported that LGP2 interacts with RIG-I or MDA5 (38–40), and may regulate the expression of ISGs through IFN production. However, these results suggest that LGP2 and TRBP are not involved in activation of the antiviral innate immune response during SeV infection. In the RNA silencing pathway, LGP2 represses RNA silencing directed by TRBP-bound miRNAs and upregulates their target genes (15). TRBP-bound miRNA activities are expected to be repressed during SeV infection in WT cells compared to mock-treated cells. By contrast, it is expected that no significant differences in such miRNA activities would be observed between mock-treated or SeV-infected LGP2$^{-/-}$ or TRBP$^{-/-}$ cells. Thus,

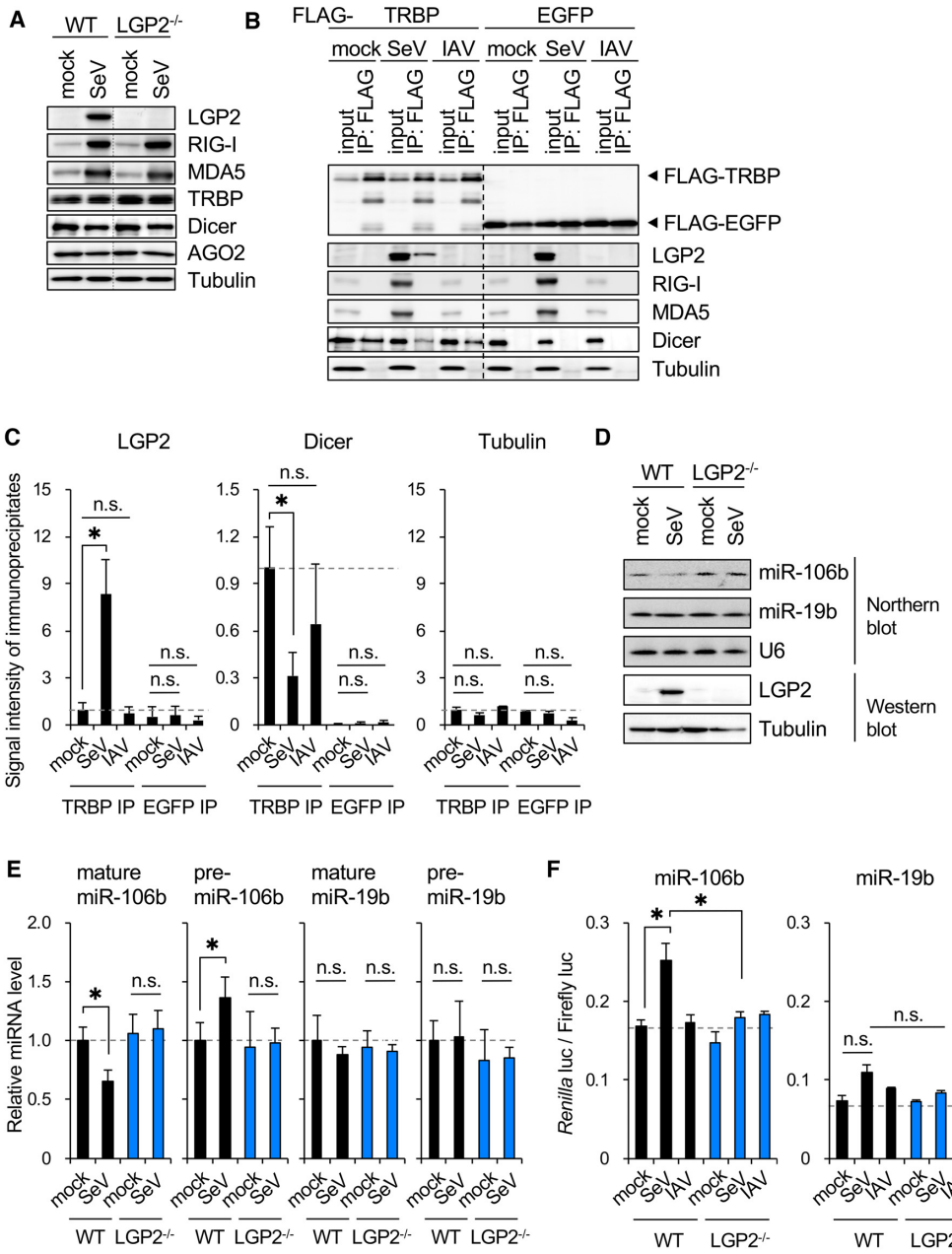

Figure 2. LGP2 interacts with TRBP and represses RNA silencing during SeV infection. (**A**) Western blots of endogenous RLRs (LGP2, RIG-I and MDA5), RNA silencing factors (TRBP, Dicer and AGO2), and control tubulin using mock-treated or SeV-infected WT or LGP2$^{-/-}$ cells at 14 h following virus infection. (**B**) Immunoprecipitation of LGP2 with TRBP. Plasmids encoding FLAG-TRBP or FLAG-EGFP were transfected into HeLa WT cells and immunoprecipitation was performed with anti-FLAG-antibody at 14 h following virus infection. (**C**) The quantified signal intensities of immunoprecipitates in Figure 2B. *P*-values were as follows. For LGP2 intensities, mock vs SeV and mock vs IAV in TRBP IP samples were 0.011 and 0.57, respectively; mock vs SeV and mock versus IAV in EGFP IP samples were 0.91 and 0.69, respectively. For Dicer intensities, mock versus SeV and mock vs IAV in TRBP IP samples were 0.032 and 0.38, respectively; mock vs SeV and mock versus IAV in EGFP IP samples were 0.34 and 0.35, respectively. For tubulin intensities, mock versus SeV and mock versus IAV in TRBP IP samples were 0.06 and 0.53, respectively; mock versus SeV and mock versus IAV in EGFP IP samples were 0.18 and 0.09, respectively. (**D**) Northern blotting was performed using mock-treated or SeV-infected WT or LGP2$^{-/-}$ cells, and endogenous mature miR-106b and miR-19b were detected. LGP2 protein was detected by western blot. The cells were collected at 14 h following virus infection. U6 and Tubulin were used as RNA and protein controls, respectively. (**E**) Relative RNA levels of the mature and precursor miR-106b or miR-19b in mock-treated and SeV infected cells, respectively. The cells were collected at 14 h following virus infection. *P*-values of mock versus SeV were as follows. For mature miR-106b, 0.00045 in WT cells; 0.70 in LGP2$^{-/-}$ cells. For pre-miR-106b, 0.024 in WT; 0.86 in LGP2$^{-/-}$. For mature miR-19b, 0.33 in WT; 0.66 in LGP2$^{-/-}$. For pre-miR-19b, 0.85 in WT; 0.92 in LGP2$^{-/-}$. (**F**) RNA silencing activity assay using a dual luciferase reporter in WT or LGP2$^{-/-}$ cells. The sensor plasmid for miRNA activity encoding the target sequence of miR-106b or miR-19b in the 3′UTR of *Renilla* luciferase and plasmid encoding firefly luciferase (internal control) were co-transfected into WT or LGP2$^{-/-}$ cells, and relative luciferase activity (*Renilla* luciferase/firefly luciferase) was determined. The cells were collected at 14 h following virus infection. *P*-values were as follows. For miR-106b, mock versus SeV in WT cells was 0.016; WT versus LGP2$^{-/-}$ by SeV infection was 0.0028. For miR-19b, mock vs SeV in WT cells was 0.17; WT versus LGP2$^{-/-}$ by SeV infection was 0.16. The mean values and standard deviations of the results of three independent experiments were shown. *P*-values were determined by Student's *t*-test (*$P < 0.05$).

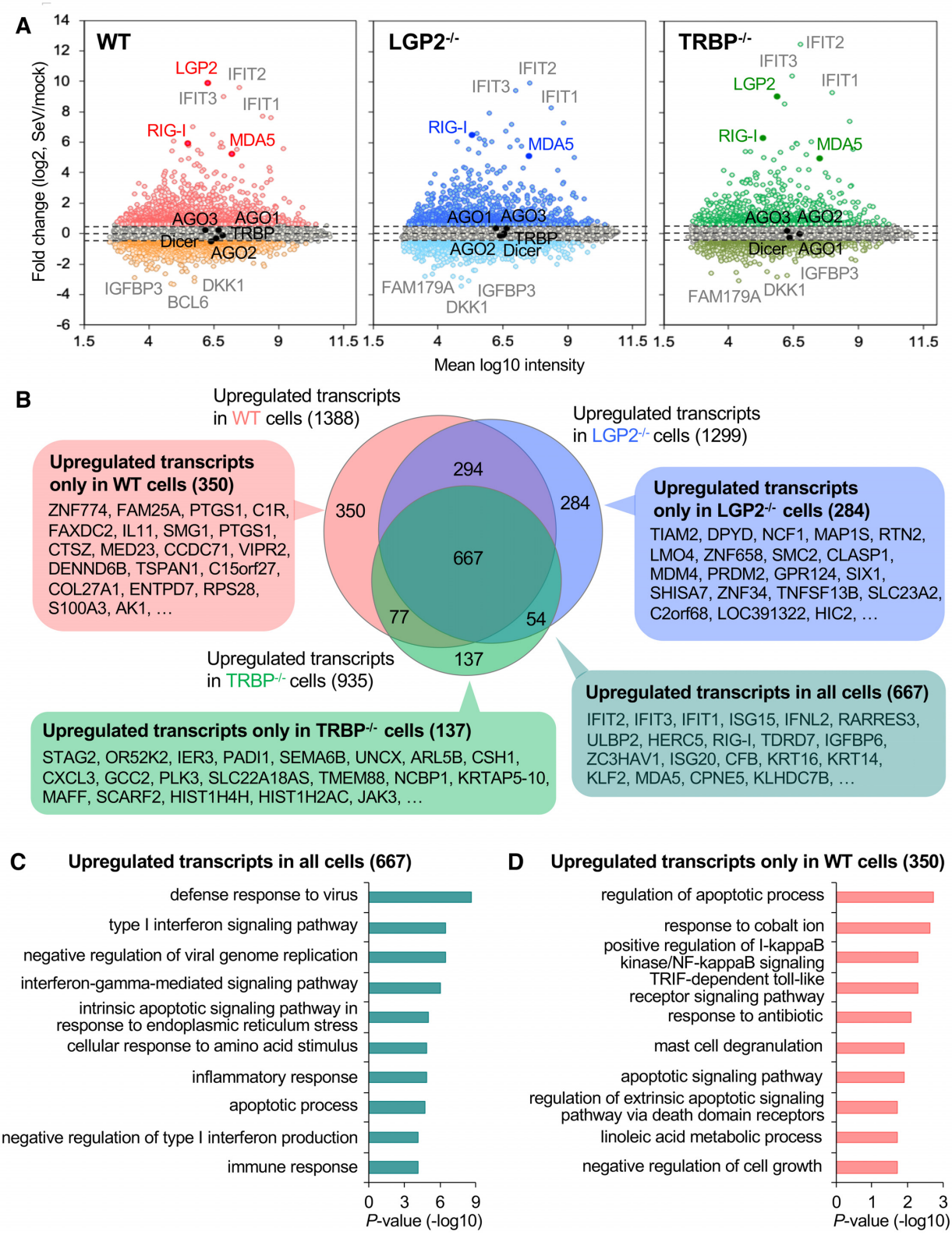

Figure 3. LGP2-TRBP interaction upregulates apoptosis regulatory genes during SeV infection. (**A**) MA plots of SeV-infected WT, LGP2$^{-/-}$ or TRBP$^{-/-}$ cells at 14 h following virus infection. The upregulated transcripts (pink, blue, or green) or downregulated transcripts (orange, light blue, or dark green) in SeV-infected cells compared with mock-treated cells indicated with different colors. (**B**) Venn diagram of upregulated transcripts during SeV infection in WT, LGP2$^{-/-}$ or TRBP$^{-/-}$ cells. The top 20 transcripts upregulated in each cell are shown in speech bubbles. (**C**) Gene ontology analysis of commonly upregulated transcripts in WT, LGP2$^{-/-}$ or TRBP$^{-/-}$ cells during SeV infection. (**D**) Gene ontology analysis of transcripts upregulated in WT cells, but not in LGP2$^{-/-}$ or TRBP$^{-/-}$ cells, during SeV infection.

their target genes should be upregulated in WT cells, but not in LGP2$^{-/-}$ or TRBP$^{-/-}$ cells, during SeV infection. The percentage of genes targeted by at least one of TRBP-bound miRNAs (sequence read enrichment by immunoprecipitation > 10) (15) in 350 transcripts upregulated only in WT cells was 72.9% (255/350 transcripts), although that of TRBP-non-bound miRNAs (sequence read enrichment by immunoprecipitation < 1/3) (15) was 16% (56/350 transcripts), when predicted with TargetScan. GO analysis of the 350 transcripts upregulated only in WT cells revealed that the enriched GO terms were related to apoptosis: regulation of apoptotic process, apoptotic signaling pathway, and regulation of extrinsic apoptotic signaling pathway via death domain receptor (Figure 3D and Supplementary Table S5), indicating that LGP2 may upregulate apoptosis regulatory genes by modulating RNA silencing directed by TRBP-bound miRNAs. By contrast, GO analysis of the 284 transcripts upregulated only in LGP2$^{-/-}$ cells revealed that regulation of cyclin-dependent protein serine/threonine kinase activity and others was enriched (Supplementary Figure S3A and Table S6), and the enriched GO terms of the 137 transcripts upregulated only in TRBP$^{-/-}$ cells were chromatin silencing and others (Supplementary Figure S3B and Table S7). GO terms related to positive regulation of apoptosis were not enriched in the upregulated transcripts in either LGP2$^{-/-}$ or TRBP$^{-/-}$ cells. In addition, the enriched GO terms of the 711 transcripts commonly downregulated in all cells included mitochondrion organization, negative regulation of transcription from RNA polymerase II promoter, or positive regulation of cell proliferation (Supplementary Figure S2B and Table S8). This result may indicate that the IFN response affects cell proliferation or growth. The 531 transcripts downregulated only in WT cells were enriched in ribosome biogenesis or rRNA processing (Supplementary Figure S2C and Table S9), suggesting the possibility that translational machinery is affected by LGP2-TRBP interaction. Furthermore, the 222 transcripts downregulated only in LGP2$^{-/-}$ cells were enriched in negative regulation of gluconeogenesis (Supplementary Figure S2D and Table S10), and the 206 transcripts downregulated only in TRBP$^{-/-}$ cells were enriched in positive regulation of endothelial cell proliferation (Supplementary Figure S2E and Table S11). Summarizing the above, both LGP2 and TRBP may regulate various functions without interacting with each other. However, our gene expression profiling suggested that apoptosis regulatory genes might be major molecules commonly modulated by LGP2 and TRBP during SeV infection.

LGP2 enhances cell death through activation of caspases during SeV infection

To verify whether LGP2 regulates apoptosis during SeV infection, we used SeV or IAV (negative control) to infect WT, LGP2$^{-/-}$ or TRBP$^{-/-}$ cells, and measured their cell viabilities for 3 days following infection (Figure 4A and B, left panels). On the first day following SeV infection, the cell viabilities of WT, LGP2$^{-/-}$ and TRBP$^{-/-}$ cells were 29.5 ± 2.9%, 47.1 ± 6.7% and 24.8 ± 2.1%, respectively (Figure 4A, right panel). The cell viability of WT cells was 0.6 times lower than that of LGP2$^{-/-}$ cells, suggesting that

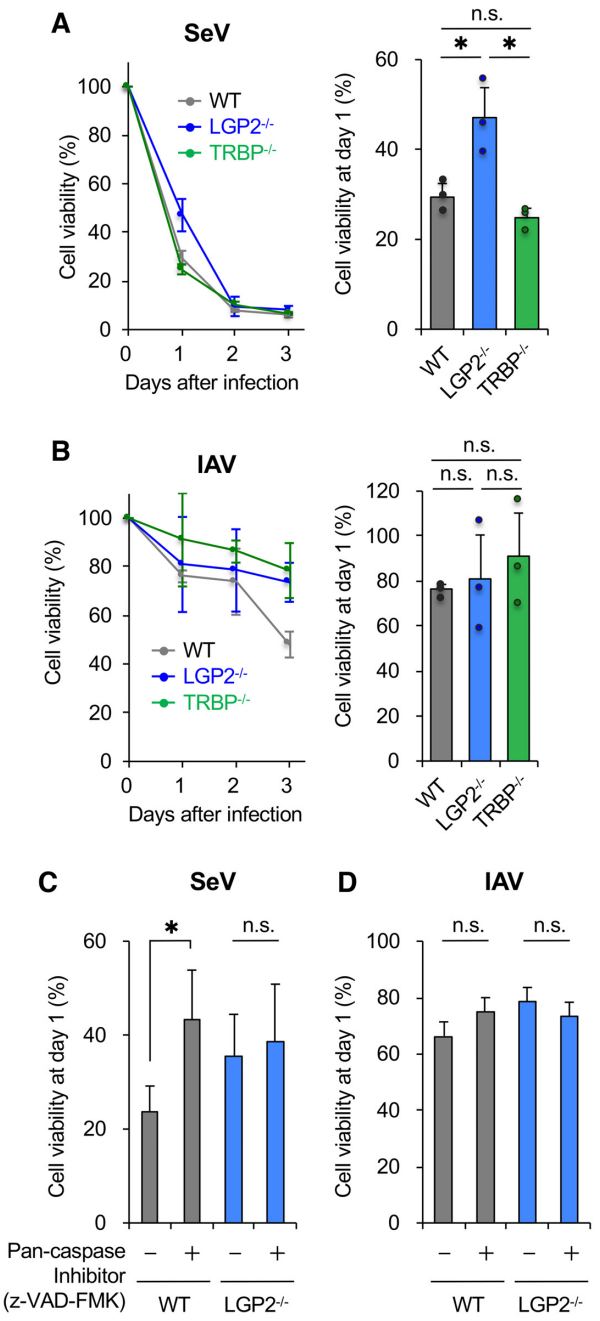

Figure 4. LGP2 enhances apoptosis through the activation of caspases during SeV infection. (**A**) Cell viabilities of SeV-infected WT, LGP2$^{-/-}$ or TRBP$^{-/-}$ cells. Mock-treated or SeV-infected cells were collected in Trypsin-EDTA and stained with Trypan Blue for cell counting. Cell viabilities of virus-infected cells normalized to that of mock-treated cells were determined. *P*-value of WT versus LGP2$^{-/-}$ was 0.027; WT versus TRBP$^{-/-}$ was 0.14; LGP2$^{-/-}$ versus TRBP$^{-/-}$ was 0.011. (**B**) Cell viabilities of IAV-infected WT, LGP2$^{-/-}$ or TRBP$^{-/-}$ cells. *P*-value of WT versus LGP2$^{-/-}$ was 0.74; WT versus TRBP$^{-/-}$ was 0.33; LGP2$^{-/-}$ versus TRBP$^{-/-}$ was 0.63. (**C**) Cell viabilities of SeV-infected WT or LGP2$^{-/-}$ cells with or without pan-caspase-inhibitor (z-VAD-FMK). *P*-value of without versus with z-VAD-FMK in WT cells was 0.0048; that in LGP2$^{-/-}$ cells was 0.66. (**D**) Cell viabilities of IAV-infected WT or LGP2$^{-/-}$ cells with or without z-VAD-FMK. *P*-value of without versus with z-VAD-FMK in WT cells was 0.22; that in LGP2$^{-/-}$ cells was 0.48. The mean values and standard deviations of the results of three independent experiments were shown. *P*-values were determined by Student's *t*-test (*P < 0.05).

LGP2 induced by IFN enhanced cell death through interaction with TRBP to upregulate apoptosis-related genes in WT cells during SeV infection. However, the cell viability of TRBP$^{-/-}$ cells was the lowest. In TRBP$^{-/-}$ cells, maturation of TRBP-bound pre-miRNAs is considered to be inhibited. Thus, the inhibitory effect of pre-miRNA maturation during SeV infection might not affect the cell viability. During IAV infection, the cell viabilities of WT, LGP2$^{-/-}$, and TRBP$^{-/-}$ cells were 76.0 ± 2.5%, 80.9 ± 19.6% and 91.1 ± 19.2%, respectively (Figure 4B, right panel), and there were no significant differences. Thus, neither LGP2 nor TRBP affected cell viability during IAV infection.

Caspases are crucial mediators of apoptotic cell death. To examine whether LGP2 enhances cell death through the activation of caspases, we measured the cell viabilities of SeV- or IAV-infected cells with or without the anti-apoptotic agent pan-caspase inhibitor, z-VAD-FMK (Figure 4C and D). The cell viability of WT cells on the first day following SeV infection was 23.7 ± 5.5%, but was increased to 43.1 ± 10.7% by the addition of z-VAD-FMK (Figure 4C, gray bars), suggesting that the cell death was induced through caspase activation. By contrast, the cell viability of SeV-infected LGP2$^{-/-}$ cells showed no significant difference with (38.6 ± 12.2%) or without (35.5 ± 8.9%) z-VAD-FMK (Figure 4C, blue bars). Furthermore, z-VAD-FMK had no significant effect during IAV infection in WT or LGP2$^{-/-}$ cells (Figure 4D). These results suggest that LGP2 enhances cell death through the activation of various caspases during SeV infection.

LGP2-TRBP interaction represses the expression of miR-106b and upregulates the expression of caspases-2, -8, -3 and -7

To examine whether LGP2 enhances apoptotic cell death through caspase activation via interaction with TRBP, we retrieved the target sequences of TRBP-bound miRNAs from caspase genes. Usually, a miRNA target sequence is known to have complementarity to its seed region, which is situated at positions 2–8 or 2–7 from the 5′ end of the miRNA (41). As shown in Figure 2D–F, LGP2 repressed both the maturation of miR-106b and its RNA silencing activity during SeV infection. We then searched for its target sequences in the 3′UTRs of both initiator caspases (caspases-2, -8, -9 and -10) and executioner caspases (caspases-3, -6 and -7), and found multiple candidate sites (Supplementary Figure S4). To examine whether miR-106b represses these caspases, the expression levels of each caspase were measured in mock-treated or SeV-infected WT or LGP2$^{-/-}$ cells with or without miR-106b overexpression (Figure 5A and B). qRT-PCR analysis showed that caspase-2, -8, -3 and -7 mRNAs were upregulated in WT cells during SeV infection (Figure 5A). If the upregulation of caspases-2, -8, -3 and -7 in WT cells is caused by the decreased miR-106b activity during SeV infection, it is expected that miR-106b overexpression would downregulate their mRNA levels in WT cells. The results showed that miR-106b overexpression downregulated the expression levels of caspases-2, -8, -3 and -7 in WT cells, but not in LGP2$^{-/-}$ cells, during SeV infection (Figure 5A), indicating that caspases-2, -8, -3 and -7 are direct or indirect targets of miR-106b. By contrast, the mRNA levels of caspases-9, -10, and -6, were not upregulated in WT cells, and accordingly miR-106b overexpression had no significant effect on their expression in either WT or LGP2$^{-/-}$ cells (Figure 5B), suggesting that caspases-9, -10 and -6 are not the targets of miR-106b or other regulatory miRNAs are needed to exert a full effect on these UTRs.

Caspase-2 and -8 are initiator caspases whose activation are important for initiation of apoptosis, and these activations induce cleavage of downstream executioner caspases. To examine whether caspases-2 or -8 are regulated by miR-106b directly or indirectly, we constructed reporter plasmids encoding the *Renilla* luciferase CDS with the 3′UTR of caspase-2 or -8 (Figure 5C). WT or mutated plasmids (mt), in which three nucleotides in each predicted miR-106b target site were deleted by site-directed mutagenesis so as not to be recognized as miR-106b target sites, were transfected with a plasmid encoding firefly luciferase (internal control) into WT cells with or without miR-106b inhibitor (TuD-miR-106b). The cells were collected 1 day after transfection and *Renilla* luciferase activities normalized to that of firefly luciferase (*Renilla* luciferase/firefly luciferase) were determined. TuD-miR-106b enhanced relative luciferase activity of CASP-2-3′UTR-WT compared to that of CASP-2-3′UTR-mt, in which the miR-106b target site was mutated (Figure 5D), suggesting that miR-106b represses caspase-2 directly through its miR-106b target sites in 3′UTR. Furthermore, TuD-miR-106b showed no significant effect on the expression of psiCHECK-CASP-8-3′UTR-WT or psiCHECK-CASP-8-3′UTR-mt, although miR-106b overexpression reduced caspase-8 mRNA levels (Figure 5A). This may indicate that caspase-8 has non-canonical target sites in its CDS. Alternatively, caspase-8 may be indirectly regulated by miR-106. Furthermore, we measured the mRNA levels of caspase-2 by qRT-PCR in WT and LGP2$^{-/-}$ cells, respectively, at 0, 6, 10, 14, 18 and 24 h following SeV infection (Supplementary Figure S5). The results showed that mRNA level of caspase-2 was upregulated at 6 h following SeV infection in both WT and LGP2$^{-/-}$ cells, but that in WT cells were upregulated strongly than that in LGP2$^{-/-}$ cells after 14 h. These results demonstrated that caspase-2 transcript was upregulated concurring with the reduction of miRNA-106b.

Finally, we examined whether LGP2 enhances cell death by repressing miR-106b activity during SeV infection. The cell viability of SeV-infected WT cells was 33.4 ± 3.1% on the first day following infection, but was rescued to 46.1 ± 4.7% by miR-106b overexpression (Figure 5E, gray bars). By contrast, the cell viability of SeV-infected LGP2$^{-/-}$ cells showed no significant effect by miR-106b overexpression (48.3 ± 1.9% versus 48.6 ± 2.5%) (Figure 5E, blue bars). Furthermore, the miR-106b inhibitor TuD-miR-106b showed no significant effect on the cell viabilities of the SeV-infected WT cells (34.5 ± 7.3% versus 33.1 ± 3.2%) (Figure 5F, gray bars), but that of SeV-infected LGP2$^{-/-}$ cells tended to be decreased by TuD-miR-106b (from 50.3 ± 12.2% to 37.8 ± 3.94%) (Figure 5F, blue bars), suggesting that LGP2 enhances cell death by repressing miR-106b activity during SeV infection.

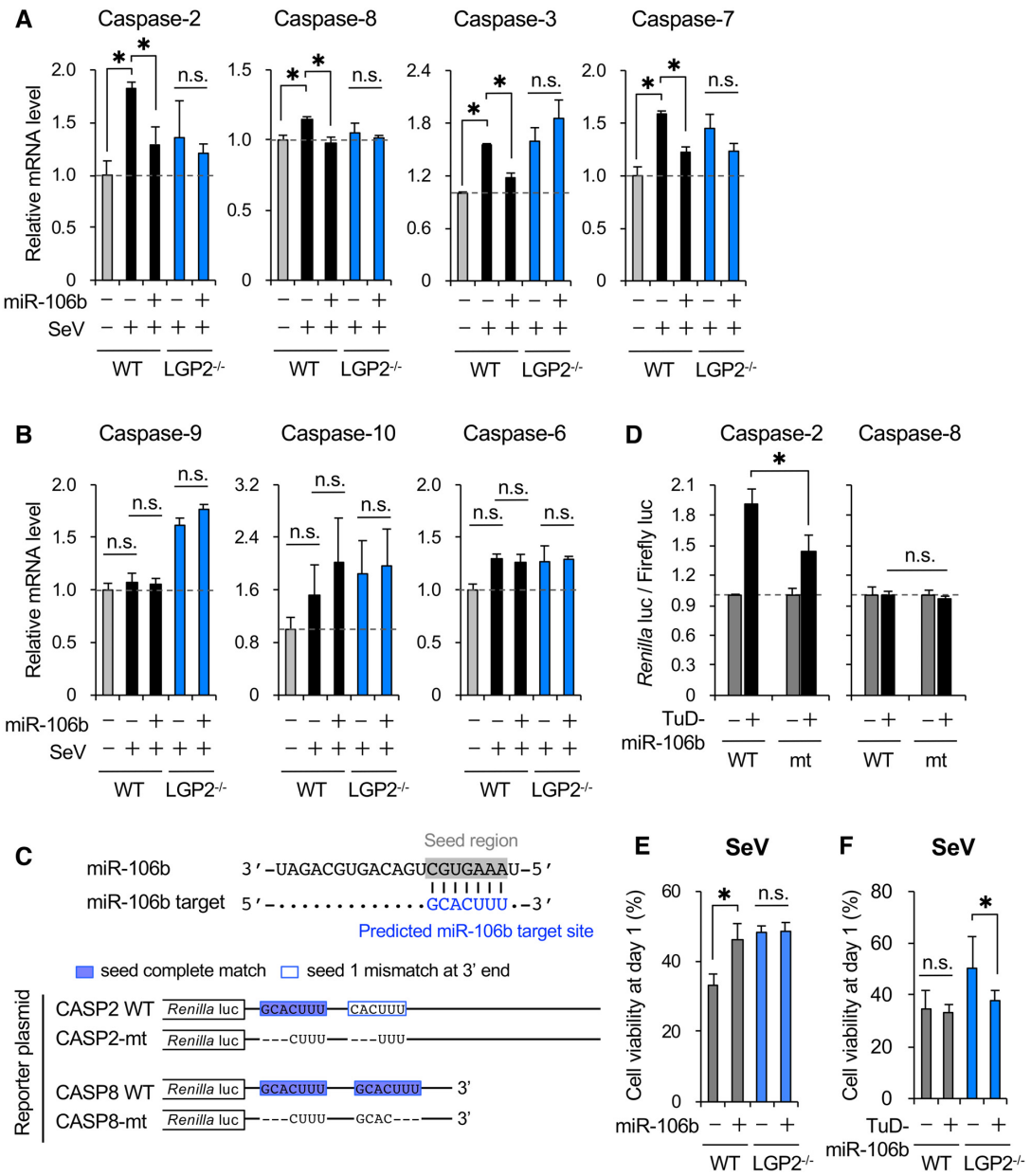

Figure 5. LGP2 upregulates caspases-2, 8, -3 and -7 mediated by miR-106b. (**A**) Relative mRNA levels of caspases-2, -8, -3 and -7 in mock-treated or SeV-infected WT or LGP2$^{-/-}$ cells with or without miR-106b overexpression quantified by qRT-PCR. The cells were collected at 14 h following viral infection. *P*-values were as follows. For caspase-2, mock versus SeV in WT cells was 0.0015; without versus with miR-106b in WT and LGP2$^{-/-}$ cells were 0.014 and 0.59, respectively. For caspase-8, mock versus SeV in WT cells was 0.0045; without versus with miR-106b in WT and LGP2$^{-/-}$ cells were 0.005 and 0.52, respectively. For caspase-3, mock versus SeV in WT cells was 0.0000034; without versus with miR-106b in WT and LGP2$^{-/-}$ cells were 0.001 and 0.23, respectively. For caspase-7, mock versus SeV in WT cells was 0.00086; without versus with miR-106b in WT and LGP2$^{-/-}$ cells were 0.001 and 0.12, respectively. (**B**) Relative mRNA levels of caspases-9, -10 and -6 in mock-treated or SeV-infected WT or LGP2$^{-/-}$ cells with or without miR-106b overexpression quantified by qRT-PCR. The cells were collected at 14 h following virus infection. *P*-values were as follows. For caspase-9, mock versus SeV in WT cells was 0.35; without versus with miR-106b in WT and LGP2$^{-/-}$ cells were 0.80 and 0.061, respectively. For caspase-10, mock versus SeV in WT cells was 0.22; without versus with miR-106b in WT and LGP2$^{-/-}$ cells were 0.44 and 0.83, respectively. For caspase-6, mock versus SeV in WT cells was 0.12; without versus with miR-106b; in WT and LGP2$^{-/-}$ cells were 0.080 and 0.086, respectively. (**C**) Schematic diagram of reporter plasmids encoding *Renilla* luciferase with the 3′UTR of caspase-2 or -8. Predicted miR-106b target sites with complementarities with nucleotides 2–8 in the 3′UTR are shown as blue boxes; and those with complementarities with nucleotides 2–7 are shown as white boxes. (**D**) Dual luciferase reporter assay of predicted miR-106b target sites on the 3′UTR of caspase-2 or -8 in WT cells. The reporter plasmids encoding *Renilla* luciferase with the 3′UTR of caspase-2 or -8 and plasmid encoding firefly luciferase (internal control) were co-transfected into WT cells, and the relative luciferase activity (*Renilla* luciferase/firefly luciferase) was determined. The cells were collected 1 day after transfection. *P*-values for caspase-2 and caspase-8 were 0.026 and 0.55, respectively. (**E**) Cell viabilities of SeV-infected WT or LGP2$^{-/-}$ cells with or without miR-106b overexpression. *P*-values for WT and LGP2$^{-/-}$ cells were 0.033 and 0.90, respectively. (**F**) Cell viabilities of SeV-infected WT or LGP2$^{-/-}$ cells with or without miR-106b inhibitor (TuD-miR-106b). The cells were collected 1 day following virus infection. *P*-value for WT cells was 0.71; that for LGP2$^{-/-}$ was 0.055, which was not statistically significant level but considered to be biologically meaningful. The mean values and standard deviations of the results of three independent experiments were shown. *P*-values were determined by Student's *t*-test.

DISCUSSION

In this report, we revealed the biological implication of modulation of RNA silencing by LGP2 induction during viral infection (Figure 6). Infection with SeV, a negative-sense single-stranded RNA virus recognized by RIG-I, induced IFN production and abundant expression of LGP2 protein via positive-feedback regulation of IFN (Figure 1). The highly upregulated LGP2 interacted with TRBP, and TRBP competitively released its bound pre-miRNAs, such as miR-106b, resulting in the reduction of mature miRNA levels (Figure 2). Furthermore, gene expression profiling analysis revealed that the possible target genes regulated by LGP2 through the modulation of RNA silencing machinery were apoptosis regulatory genes (Figure 3). LGP2 enhanced cell death during SeV infection through activation of caspases (Figure 4), and the expression levels of caspases-2, -8, -3 and -7 were downregulated through the increase of miR-106b during SeV infection (Figure 5). Consistent with our results, several previous reports have demonstrated the anti-apoptotic function of miR-106b in lung cancer cells, vascular endothelial cells, and glioma cells (42–44), and the deletion of a miRNA cluster including miR-106b induced lethality in mice (45). In these cancer cell lines, miR-106b enhances cell proliferation and inhibits apoptosis by targeting B-cell translocation gene 3 (BTG3) or phosphatase and tensin homolog deleted from chromosome 10 (PTEN), which functions as a tumor suppressor. Furthermore, increased miR-106b levels and tumorigenesis are correlated (42–44). However, the molecular mechanism by which miR-106b regulates tumorigenesis was unclear. In this report, we determined the functional machinery of miR-106b in apoptotic cell death during viral infection and the regulatory mechanism of miR-106b expression levels. The regulation of miR-106b by TRBP and its partner proteins may have important functions not only in virus-infected cells, but also in cancer cells, since it is reported that overexpression of TRBP induces tumorigenesis (46). It has been reported that transfection of a synthetic analog of dsRNA, polyinosinic:polycytidylic acid [poly(I:C)], induces LGP2 expression and induces cell death (47,48). Such cell death is observed both in human gastric adenocarcinoma cells, in which RIG-I and MDA5 are upregulated (47), and in neuroblastoma cells, in which RIG-I and MDA5 are downregulated (48). Thus, these results support our conclusion that LGP2 enhances apoptotic cell death by upregulating apoptosis regulatory genes during viral infection, and our findings may have revealed the molecular mechanism of enhancement of apoptosis by LGP2.

During viral infection, virus sensor proteins including TLR3 or RLRs detect viral nucleic acids in the endosome or the cytoplasm. Activation of the downstream signaling cascade induces IFN production and inhibits viral repression. On the other hand, viral infection induces apoptosis to exclude the virus-infected cells as a host defense system, but the explicit mechanism is unclear. We identified a major pathway for the induction of apoptosis in virus-infected cells through the interaction between LGP2, an RLR, and TRBP, an RNA silencing enhancer. In the previous reports, RNA silencing and RLR signaling were considered to be two independent pathways, although both pathways are commonly induced by dsRNAs in the cytoplasm. For the first time, we have demonstrated that these two pathways are not independent and their crosstalk functions as an antiviral defense system to induce apoptotic cell death during viral infection in mammalian cells. Our results suggest that IFN response is mainly regulated by RIG-I and MDA5, but apoptosis is regulated by LGP2-TRBP interaction. Thus, viral replication and cell death in virus-infected cells can be distinguished by the type of RLR involved: RIG-I/MDA5 and LGP2, respectively. The interactive regulation among RLR family proteins may reveal the selective mechanisms of virus exclusion or apoptosis.

In the type-I IFN signaling pathway, LGP2 interacts with RIG-I or MDA5 (38–40), and may regulate the expression of ISGs through IFN production. However, IFN production showed no significant difference between WT and LGP2$^{-/-}$ HeLa cells during SeV infection (Figure 1A). Since the expression level of TRBP is known to differ in various types of tissues or cells *in vivo* (37,49), it may be important factor in the regulation of IFN production. In cells with low levels of TRBP expression, the upregulated LGP2 may interact with RIG-I or MDA5 preferentially and function to induce IFN production. By contrast, in cells with moderate or high levels of TRBP expression, the upregulated LGP2 may interact preferentially with TRBP to modulate RNA silencing. Further investigations are needed to reveal the function of LGP2/TRBP interaction for IFN production during viral infection *in vivo*.

We showed that SeV infection repressed RNA silencing activity directed by endogenous miR-106b in WT cells, but not in LGP2$^{-/-}$ cells (Figure 2F, left panel). By contrast, RNA silencing activity directed by endogenous miR-19b showed no significant difference in either WT or LGP2$^{-/-}$ cells (Figure 2F, right panel). Although there were no statistical significances, Figure 2F appears to show the similar trends in effects of miR-106b and miR-19b: (i) RNA silencing activity was significantly decreased by miR-106b and slightly by miR-19b during SeV infection in WT cells and (ii) the slight reductions of RNA silencing activities during SeV and IAV infections by miR-106b and miR-19b in both WT and LGP2$^{-/-}$ cells. Seo *et al.* (50) reported that AGO2 is poly-ADP-ribosylated during viral infection, resulting in the decrease of RNAi activity. This suggests that the slight reductions of RNA silencing activities during both SeV and IAV infections may be the outcomes of AGO2 poly-ADP-ribosylation. However, SeV-mediated reduction of RNA silencing activity was significantly observed by miR-106 but not significantly and slightly by miR-19b in WT cells. Such insignificant reduction by miR-19b may be caused by a weakly predicted target sequence (a complementary sequence with nucleotides 2–7 from the 5′ end) of another TRBP-bound miRNA, miR-605, in the 3′UTR of the reporter *Renilla luciferase* gene induced by SeV infection. These results suggest that the cause of the decrease of RNAi activity by AGO2 poly-ADP-ribosylation is independent of that by LGP2-TRBP interaction.

We showed that caspase-2 is a direct target of miR-106b (Figure 5). Although we could not clarify whether caspase-8 is a direct or indirect target gene of miR-106b, caspase-2 is reported to be activated along with caspase-8 in response to multiple triggers including DNA damage, heat shock,

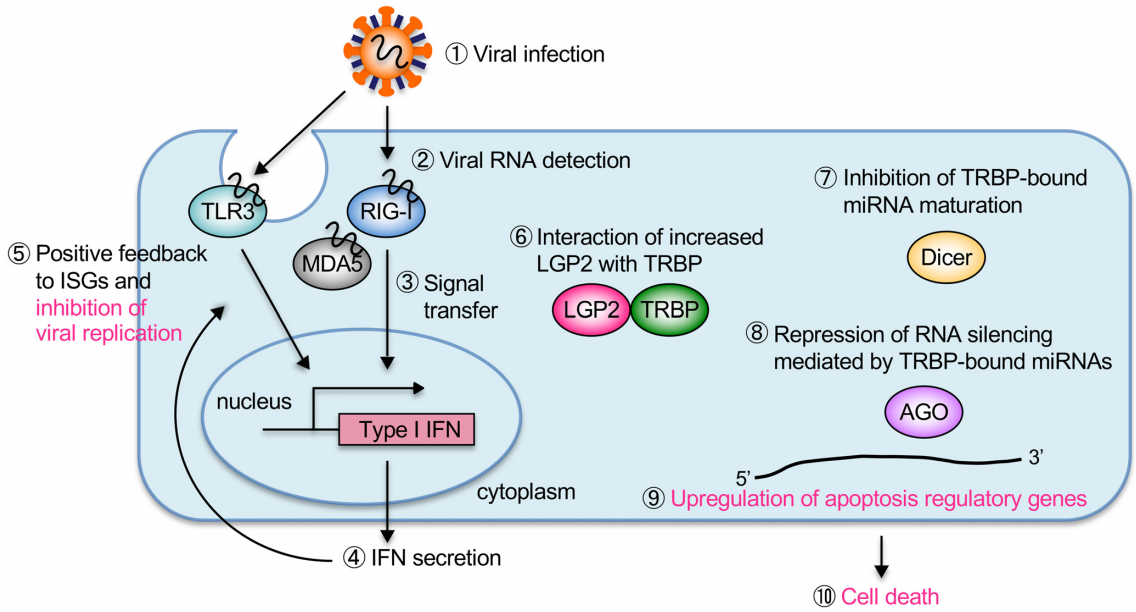

Figure 6. LGP2 virus sensor upregulates apoptosis regulatory genes and enhances apoptosis mediated by TRBP-bound miRNAs during viral infection. During viral infection, viral nucleic acids are detected by virus sensor proteins. Activated virus sensor proteins transfer the signals to downstream molecules, inducing IFN production. Secreted IFN induces the expression of ISGs and inhibits virus replication. LGP2 induced by secreted IFN interacts with the RNA silencing enhancer TRBP and inhibits TRBP-bound miRNA maturation and its RNA silencing activity, resulting in the upregulation of apoptosis regulatory genes and enhancement of apoptosis.

endoplasmic reticulum stress, and oxidative stress (51–55). The initiator caspases, caspases-2 and -8, form a complex with Fas-associated protein with death domain (FADD), and this interaction induces the downstream activation of executioner caspase-3, and finally induces apoptosis (51). Thus, LGP2 may efficiently enhance apoptosis by regulating initiator caspase(s).

We identified 40 TRBP-bound miRNAs and 10 non-TRBP-bound miRNAs by RNA sequencing of TRBP-bound miRNAs in a previous report (15). We revealed that caspase-2 is a direct target of miR-106b (Figure 5), however, caspase-2 was not upregulated during SeV infection in microarray analysis (Supplementary Table S7). By contrast, caspase-9 was not a target of miR-106b (Figure 5), but was upregulated in microarray analysis (Supplementary Table S7). The target prediction using TargetScan (56) revealed that caspase-2 has the predicted target sites of multiple TRBP-bound miRNAs (such as miR-10, miR-31, miR-708, miR-378, miR-605, miR-766, miR-345 and miR-324) and caspase-9 also has the predicted target sites of the miRNAs (such as miR-140, miR-590, miR-10, miR-25, miR-378, miR-708, miR-340, miR-766, miR-605, miR-126, miR-582 and miR-345). These results may indicate that the simultaneous regulation of multiple TRBP-bound miRNAs creates a systematically-regulated gene expression network in virus-infected cells, and caspases-2 and -9 can be regulated simultaneously by multiple TRBP-bound miRNAs.

In summary, we found that LGP2 upregulates apoptosis regulatory genes mediated by the repression of TRBP-bound miRNAs and enhances apoptosis during SeV infection. The crosstalk between RNA silencing and RLR signaling functions as an antiviral defense system in mammalian cells.

DATA AVAILABILITY

Microarray data is registered with GEO, accession number GSE135547.

SUPPLEMENTARY DATA

Supplementary Data are available at NAR Online.

ACKNOWLEDGEMENTS

We thank Dr H. Iba and Dr T. Haraguchi for kindly providing microRNA inhibitor (TuD-decoy). T.T. and K.U.-T. designed the study at first, and T.T., Y.N., K.O, M.Y. and K.U.-T. discussed the methods, results, and the experimental plans. T.T., Y.N. and K.O. performed the experiments and T.T. analyzed microarray data. The manuscript was drafted by T.T. and K.U.-T. and T.T., M.Y., and K.U.-T. were involved in reviewing the manuscript. All authors read and approved the final manuscript.

FUNDING

Ministry of Education, Culture, Sports, Science and Technology of Japan [21310123, 21115004, 15H04319, 16H14640, 221S0002, 16H06279 to K.U.-T., 15K19124, 18K15178 to T.T.]; Ichiro Kanehara Foundation, the Inamori Foundation, the Uehara Memorial Foundation, and Japan Science and Technology Agency (to T.T.); Japan Health & Research Institute and the Kurata Grant awarded by the Hitachi Global Foundation (to K.U.-T.); Joint Usage/Research Program of Medical Mycology Research Center, Chiba University [14-14, 15-16, 16-1, 17-15, 18-11, 19-1 to T.T., K.O., M.Y. and K.U.-T.]. Funding for open

access charge: The Ministry of Education, Culture, Sports, Science and Technology of Japan.
Conflict of interest statement. None declared.

REFERENCES

1. Wilson,R.C. and Doudna,J.A. (2013) Molecular mechanisms of RNA interference. *Annu. Re. Biophys.*, **42**, 217–239.
2. Kozomara,A. and Griffiths-Jones,S. (2014) miRBase: annotating high confidence microRNAs using deep sequencing data. *Nucleic Acids Res.*, **42**, D68–D73.
3. Lee,Y., Kim,M., Han,J., Yeom,K.H., Lee,S., Baek,S.H. and Kim,V.N. (2004) MicroRNA genes are transcribed by RNA polymerase II. *EMBO J.*, **23**, 4051–4060.
4. Lee,Y., Ahn,C., Han,J., Choi,H., Kim,J., Yim,J., Lee,J., Provost,P., Rådmark,O., Kim,S. *et al.* (2003) The nuclear RNase III Drosha initiates microRNA processing. *Nature*, **425**, 415–419.
5. Han,J., Lee,Y., Yeom,K.H., Kim,Y.K., Jin,H. and Kim,V.N. (2004) The Drosha-DGCR8 complex in primary microRNA processing. *Genes Dev.*, **18**, 3016–3027.
6. Yi,R., Qin,Y., Macara,I.G. and Cullen,B.R. (2003) Exportin-5 mediates the nuclear export of pre-microRNAs and short hairpin RNAs. *Genes Dev.*, **17**, 3011–3016.
7. Lund,E., Güttinger,S., Calado,A., Dahlberg,J.E. and Kutay,U. (2004) Nuclear export of microRNA precursors. *Science*, **303**, 95–98.
8. Doi,N., Zenno,S., Ueda,R., Ohki-Hamazaki,H., Ui-Tei,K. and Saigo,K. (2003) Short-interfering-RNA-mediated gene silencing in mammalian cells requires Dicer and eIF2C translation initiation factors. *Curr. Biol.*, **13**, 41–46.
9. Liu,J., Carmell,M.A., Rivas,F.V., Marsden,C.G., Thomson,J.M., Song,J.J., Hammond,S.M., Joshua-Tor,L. and Hannon,G.J. (2004) Argonaute2 is the catalytic engine of mammalian RNAi. *Science*, **305**, 1437–1441.
10. Rivas,F.V., Tolia,N.H., Song,J.J., Aragon,J.P., Liu,J., Hannon,G.J. and Joshua-Tor,L. (2005) Purified Argonaute2 and an siRNA form recombinant human RISC. *Nat. Struct. Mol. Biol.*, **12**, 340–349.
11. Gatignol,A., Buckler-White,A., Berkhout,B. and Jeang,K.T. (1991) Characterization of a human TAR RNA-binding protein that activates the HIV-1 LTR. *Science*, **251**, 1597–1600.
12. Chendrimada,T.P., Gregory,R.I., Kumaraswamy,E., Norman,J., Cooch,N., Nishikura,K. and Shiekhatter,R. (2005) TRBP recruits the Dicer complex to Ago2 for microRNA processing and gene silencing. *Nature*, **436**, 740–744.
13. Haase,A.D., Jaskiewicz,L., Zhang,H., Lainé,S., Sack,R., Gatignol,A. and Fillipowicz,W. (2005) TRBP, a regulator of cellular PKR and HIV-1 virus expression, interacts with Dicer and functions in RNA silencing. *EMBO Rep.*, **6**, 961–967.
14. Liu,Z., Wang,J., Cheng,H., Ke,X., Sun,L., Zhang,Q.C. and Wang,H.W. (2018) Cryo-EM structure of human dicer and its complexes with a Pre-miRNA substrate. *Cell*, **173**, 1191–1203.
15. Takahashi,T, Nakano,Y, Onomoto,K, Murakami,F, Komori,C, Suzuki,Y, Yoneyama,M and Ui-Tei,K. (2018) LGP2 virus sensor regulates gene expression network mediated by TRBP-bound microRNAs. *Nucleic Acids Res.*, **46**, 9134–9147.
16. Yoneyama,M. and Fujita,T. (2010) Recognition of viral nucleic acids in innate immunity. *Rev. Med. Virol.*, **20**, 4–22.
17. Yoneyama,M., Onomoto,K., Jogi,M., Akaboshi,T. and Fujita,T. (2015) Viral RNA detection by RIG-I-like receptors. *Curr. Opin. Immunol.*, **32**, 48–53.
18. Alexopoulou,L., Holt,A.C., Medzhitov,R. and Flavell,R.A. (2001) Recognition of double-stranded RNA and activation of NF-kappaB by Toll-like receptor 3. *Nature*, **413**, 732–738.
19. Yoneyama,M., Kikuchi,M., Natsukawa,T., Shinobu,N., Imaizumi,T., Miyagishi,M., Taira,K., Akira,S. and Fujita,T. (2004) The RNA helicase RIG-I has an essential function in double-stranded RNA-induced innate antiviral responses. *Nat. Immunol.*, **5**, 730–737.
20. Yoneyama,M., Kikuchi,M., Matsumoto,K., Imaizumi,T., Miyagishi,M., Taira,K., Foy,E., Loo,Y.M., Gale,M.Jr, Akira,S. *et al.* (2005) Shared and unique functions of the DExD/H-box helicases RIG-I, MDA5, and LGP2 in antiviral innate immunity. *J. Immunol.*, **175**, 2851–2858.
21. Hornung,V., Ellegast,J., Kim,S., Brzózka,K., Jung,A., Kato,H., Poeck,H., Akira,S., Conzelmann,K.K., Schlee,M. *et al.* (2006) 5′-Triphosphate RNA is the ligand for RIG-I. *Science*, **314**, 994–997.
22. Pichlmair,A., Schulz,O., Tan,C.P., Näslund,T.I., Liljeström,P., Weber,F. and Reis e Sousa,C. (2006) RIG-I-mediated antiviral responses to single-stranded RNA bearing 5′-phosphates. *Science*, **314**, 997–1001.
23. Takahasi,K., Yoneyama,M., Nishihori,T., Hirai,R., Kumeta,H., Narita,R., Gale,M.Jr, Inagaki,F. and Fujita,T. (2008) Nonself RNA-sensing mechanism of RIG-I helicase and activation of antiviral immune responses. *Mol. Cell*, **29**, 428–440.
24. Wang,Y., Ludwig,J., Schuberth,C., Goldeck,M., Schlee,M., Li,H., Juranek,S., Sheng,G., Micura,R., Tuschl,T. *et al.* (2010) Structural and functional insights into 5′-ppp RNA pattern recognition by the innate immune receptor RIG-I. *Nat. Struct. Mol. Biol.*, **17**, 781–787.
25. Goubau,D., Schlee,M., Deddouche,S., Pruijssers,A.J., Zillinger,T., Goldeck,M., Schuberth,C., Van der Veen,A.G., Fujimura,T., Rehwinkel,J. *et al.* (2014) Antiviral immunity via RIG-I-mediated recognition of RNA bearing 5′-diphosphates. *Nature*, **514**, 372–375.
26. Kato,H., Takeuchi,O., Mikamo-Satoh,E., Hirai,R., Kawai,T., Matsushita,K., Hiiragi,A., Dermody,T.S., Fujita,T. and Akira,S. (2008) Length-dependent recognition of double-stranded ribonucleic acids by retinoic acid-inducible gene-I and melanoma differentiation-associated gene 5. *J. Exp. Med.*, **205**, 1601–1610.
27. Kawai,T., Takahashi,K., Sato,S., Coban,C., Kumar,H., Kato,H., Ishiim,K.J., Takeuchi,O. and Akira,S. (2005) IPS-1, an adaptor triggering RIG-I- and Mda5-mediated type I interferon induction. *Nat. Immunol.*, **6**, 981–988.
28. Seth,R.B., Sun,L., Ea,C.K. and Chen,Z.J. (2005) Identification and characterization of MAVS, a mitochondrial antiviral signaling protein that activates NF-kappaB and IRF 3. *Cell*, **122**, 669–682.
29. Vazquez,C. and Horner,S.M. (2015) MAVS coordination of antiviral innate immunity. *J. Virol.*, **89**, 6974–6977.
30. Li,Y., Basavappa,M., Lu,J., Dong,S., Cronkite,D.A., Prior,J.T., Reinecker,H.C., Hertzog,P., Han,Y., Li,W.X. *et al.* (2016) Induction and suppression of antiviral RNA interference by influenza A virus in mammalian cells. *Nat. Microbiol.*, **2**, 16250.
31. Onomoto,K., Jogi,M., Yoo,J.S., Narita,R., Morimoto,S., Takemura,A., Sambhara,S., Kawaguchi,A., Osari,S., Nagata,K. *et al.* (2012) Critical role of an antiviral stress granule containing RIG-I and PKR in viral detection and innate immunity. *PLoS One*, **7**, e43031.
32. Huang,D.W., Sherman,B.T. and Lempicki,R.A. (2009) Systematic and integrative analysis of large gene lists using DAVID bioinformatics resources. *Nat. Protoc.*, **4**, 44–57.
33. Huang,D.W., Sherman,B.T. and Lempicki,R.A. (2009) Bioinformatics enrichment tools: paths toward the comprehensive functional analysis of large gene lists. *Nucleic Acids Res.*, **37**, 1–13.
34. Talon,J., Horvath,C.M., Polley,R., Basler,C.F., Muster,T., Palese,P. and García-Sastre,A. (2000) Activation of interferon regulatory factor 3 is inhibited by the influenza A virus NS1 protein. *J. Virol.*, **74**, 7989–7996.
35. Lu,J., O'Hara,E.B., Trieselmann,B.A., Romano,P.R. and Dever,T.E. (1999) The interferon-induced double-stranded RNA activated protein kinase PKR will phosphorylate serine, threonine, or tyrosine at residue 54 in eukaryotic initiation factor 2α. *J. Biol. Chem.*, **274**, 32198–32203.
36. Dever,T.E. (2002) Gene-specific regulation by general translation factors. *Cell*, **108**, 545–556.
37. Daniels,S.M., Melendez-Peña,C.E., Scarborough,R.J., Daher,A., Christensen,H.S., El Far,M., Purcell,D.F., Lainé,S. and Gatignol,A. (2009) Characterization of the TRBP domain required for Dicer interaction and function in RNA interference. *BMC Mol. Biol.*, **10**, 38.
38. Saito,T., Hirai,R., Loo,Y.M., Owen,D., Johnson,C.L., Sinha,S.C., Akira,S., Fujita,T. and Gale,M. Jr. (2007) Regulation of innate antiviral defenses through a shared repressor domain in RIG-I and LGP2. *Proc. Natl. Acad. Sci. U.S.A.*, **104**, 582–587.
39. Takahashi,T., Nakano,Y., Onomoto,K., Yoneyama,M. and Ui-Tei,K. (2018) Virus sensor RIG-I represses RNA interference by interacting with TRBP through LGP2 in mammalian cells. *Genes (Basel)*, **9**, 511.
40. Bruns,A.M., Leser,G.P., Lamb,R.A. and Horvath,C.M. (2014) The innate immune sensor LGP2 activates antiviral signaling by

regulating MDA5-RNA interaction and filament assembly. *Mol. Cell*, **55**, 771–781.
41. Bartel,D.P. (2009) MicroRNAs: target recognition and regulatory functions. *Cell*, **136**, 215–233.
42. Wei,K., Pan,C., Yao,G., Liu,B., Ma,T., Xia,Y., Jiang,W., Chen,L. and Chen,Y. (2017) MiR-106b-5p promotes proliferation and inhibits apoptosis by regulating BTG3 in non-small cell lung cancer. *Cell Physiol. Biochem.*, **44**, 1545–1558.
43. Zhang,J., Li,S.F., Chen,H. and Song,J.X. (2016) MiR-106b-5p inhibits tumor necrosis factor-α-induced apoptosis by targeting phosphatase and tensin homolog deleted on chromosome 10 in vascular endothelial cells. *Chin. Med. J. (Engl.)*, **129**, 1406–1412.
44. Liu,F., Gong,J., Huang,W., Wang,Z., Wang,M., Yang,J., Wu,C., Wu,Z. and Han,B. (2014) MicroRNA-106b-5p boosts glioma tumorigensis by targeting multiple tumor suppressor genes. *Oncogene*, **33**, 4813–4822.
45. Ventura,A., Young,A.G., Winslow,M.M., Lintault,L., Meissner,A., Erkeland,S.J., Newman,J., Bronson,R.T., Crowley,D., Stone,J.R. *et al.* (2008) Targeted deletion reveals essential and overlapping functions of the miR-17 through 92 family of miRNA clusters. *Cell*, **132**, 875–886.
46. Benkirane,M., Neuveut,C., Chun,R.F., Smith,S.M., Samuel,C.E., Gatignol,A. and Jeang,K.T. (1997) Oncogenic potential of TAR RNA binding protein TRBP and its regulatory interaction with RNA-dependent protein kinase PKR. *EMBO J.*, **16**, 611–624.
47. Qu,J., Hou,Z., Han,Q., Zhang,C., Tian,Z. and Zhang,J. (2013) Poly(I:C) exhibits an anti-cancer effect in human gastric adenocarcinoma cells which is dependent on RLRs. *Int. Immunopharmacol.*, **17**, 814–820.
48. Lin,L.L., Huang,C.C., Wu,M.T., Hsu,W.M. and Chuang,J.H. (2018) Innate immune sensor laboratory of genetics and physiology 2 suppresses tumor cell growth and functions as a prognostic marker in neuroblastoma. *Cancer Sci.*, **109**, 3494–3502.
49. Daniels,S.M. and Gatignol,A. (2012) The multiple functions of TRBP, at the hub of cell responses to viruses, stress, and cancer. *Microbiol. Mol. Biol. Rev.*, **76**, 652–666.
50. Seo,G.J., Kincaid,R.P., Phanaksri,T., Burke,J.M., Pare,J.M., Cox,J.E., Hsiang,T.Y., Krug,R.M. and Sullivan,C.S. (2013) Reciprocal inhibition between intracellular antiviral signaling and the RNAi machinery in mammalian cells. *Cell Host Microbe.*, **14**, 435–445.
51. Thomas,C.N., Berry,M., Logan,A., Blanch,R.J. and Ahmed,Z. (2017) Caspases in retinal ganglion cell death and axon regeneration. *Cell Death Discov.*, **3**, 17032.
52. Ho,L.H., Read,S.H., Dorstyn,L., Lambrusco,L. and Kumar,S. (2008) Caspase-2 is required for cell death induced by cytoskeletal disruption. *Oncogene*, **27**, 3393–3404.
53. Tu,S., McStay,G.P., Boucher,L.M., Mak,T., Beere,H.M. and Green,D.R. (2006) In situ trapping of activated initiator caspases reveals a role for caspase-2 in heat shock-induced apoptosis. *Nat. Cell Biol.*, **8**, 72–77.
54. Sidi,S., Sanda,T., Kennedy,R.D., Hagen,A.T., Jette,C.A., Hoffmans,R., Pascual,J., Imamura,S., Kishi,S., Amatruda,J.F. *et al.* (2008) Chk1 suppresses a caspase-2 apoptotic response to DNA damage that bypasses p53, Bcl-2, and caspase-3. *Cell*, **133**, 864–877.
55. Upton,J.P., Austgen,K., Nishino,M., Coakley,K.M., Hagen,A., Han,D., Papa,F.R. and Oakes,S.A. (2008) Caspase-2 cleavage of BID is a critical apoptotic signal downstream of endoplasmic reticulum stress. *Mol. Cell Biol.*, **28**, 3943–3951.
56. Agarwal,V., Bell,G.W., Nam,J.W. and Bartel,D.P. (2015) Predicting effective microRNA target sites in mammalian mRNAs. *Elife*, **4**, e05005.